INSTITUTO SUPERIOR TÉCNICO

PROJECTO MEFT

Linearized General Relativity in Hyperboloidal Coordinates

Author:
Filipe Ficalho

Supervisor:
Prof. David Hilditch

Research work performed for the Master in Physics Engineering

at

GRIT
CENTRA

January 9, 2025

1 Introduction

When studying gravitational waves, one has to keep in mind that gravitational wave sources (like black hole mergers, neutron stars, etc.) are usually located billions of light years away from us. From the point of view of an observer on Earth, this distance is so vast that it can be approximated as being at infinity. This distance, however, is not sufficiently far away to require accounting for the cosmological constant, allowing us to model spacetime as asymptotically flat. Thus, we are interested in studying the behavior of the gravitational fields at null infinity, $\mathscr{I}$.

To do so, we must perform a conformal compactification of the spacetime, which brings $\mathscr{I}$ to a finite distance on our computational grid. This is done by working in the hyperboloidal coordinate system.

1.1 Hyperboloidal Coordinates

The hyperboloidal coordinate system, as previously mentioned, maps our previously unbonded domain to a finite one. This is done by introducing new time and radial coordinates (t, r), which are related to the spherical coordinates of Minkowski spacetime (T, R) by the transformations

$$t = T - H(R) \quad R = \frac{r}{\Omega(r)} \,, \tag{1}$$

where $H(R)$ is called the height function and $\Omega(r)$ is called the compress function, which give rize to the following Jacobian matrix:

$$\left(J^{Hyp}\right)_{\alpha'}^{\ \beta} = \begin{pmatrix} 1 & -H'(r) & 0 & 0 \\ 0 & \frac{L(r)}{\Omega^2(r)} & 0 & 0 \\ 0 & 0 & 1 & 0 \\ 0 & 0 & 0 & 1 \end{pmatrix} \,, \tag{2}$$

where $H'(r)$ denotes the derivative of the height function with respect to R written as a function of r, and $L(r)$ is defined as

$$L(r) \equiv \Omega(r) - r\,\partial_r\Omega(r) \,. \tag{3}$$

This coordinate system is particularly useful because it allows us to do the desired compactification while mantaining the characteristic speed of outgoing waves finite. Additionally, it is possible for us to choose the height and compress functions in such a way that the outgoing light speed is constant. This property can be observed in figure 1 for a specific choice of the height and compress functions. In exchange, this coordinate system makes incoming waves hard to resolve.

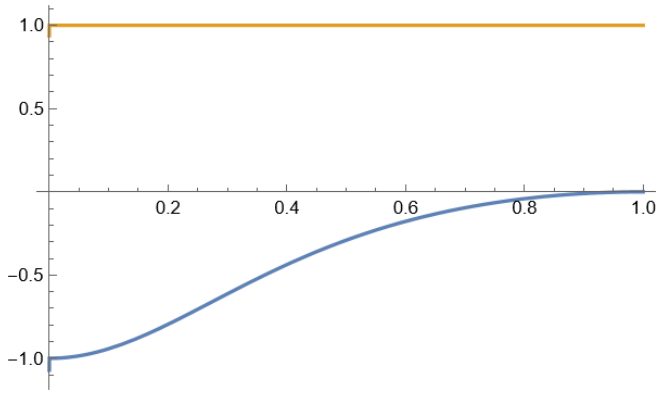

FIGURE 1: Outgoing and incoming light speeds for $H(R) = \frac{2R^2+S^2-\sqrt{4R^2S^2+S^4}}{2R}$ and $\Omega(r) = 1 - \frac{r^2}{S^2}$, with $S = 1$.

Throughout this work, we will sacrifice this very relevant property in exchange for ease of manipulation of the expressions, since the goal of this introductory work to the subject is to get accostumed with the coordinate system. The height and compress functions that will used throughout this work are

$$H(R) = \sqrt{S^2 + R^2} \quad \Omega(r) = \frac{1}{2}\left(1 - \frac{r^2}{S^2}\right) \quad , \tag{4}$$

where S is a constant that determines the size of the compactified domain. The choice of S is arbitrary, as it simply defines what point $\mathscr{I}$ will be maped to. We will set $S = 1$. As a consequence of our previous choices, we also have

$$H'(r) = \frac{2rS}{S^2+r^2} \quad L(r) = \frac{1}{2}\left(1 + \frac{r^2}{S^2}\right) . \tag{5}$$

For this choice of functions, we still have that the incoming light speed decreases as it reaches $\mathscr{I}$. However, we don't have a constant outgoing propagation speed. This can be seen in figure 2. The only implication this choice will have in our results is that the wave will take longer to reach $\mathscr{I}$ and will be slightly distorted. This is not a problem for our purposes, since on this first approach we are only interested in making sure the code converges smoothly towards the solution.

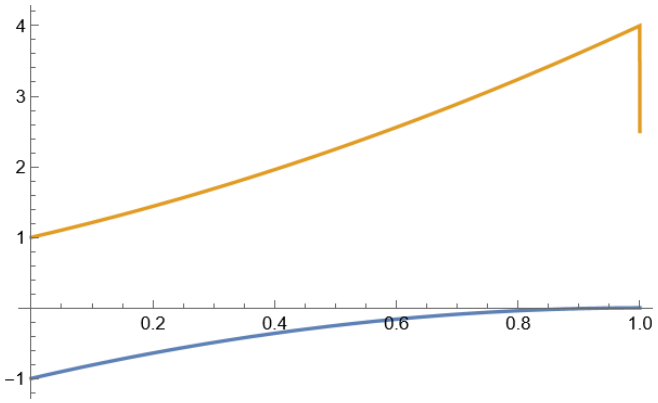

FIGURE 2: Outgoing and incoming light speeds for $H(R) = \sqrt{S^2 + R^2}$ and $\Omega(r) = \frac{1}{2}\left(1 - \frac{r^2}{S^2}\right)$, with $S = 1$.

1.2 Computational Setup

This work is a continuation of my previous work on numerical relativity. As such, the framework used here is the same as the one used in that work, with the adition of truncation error matching for the derivatives, interpolation at the boundaries and the Evans Method for regularization at the origin. The description of the base code can be found in [], and this section will elaborate on the upgrades made.

1.2.1 Truncation Error Matching

Truncation error matching is a technique used to improve the accuracy of the numerical solution by matching the truncation error of the finite difference scheme used on the boundaries to the truncation error of the one used in the interior of our computational domain. This is done by using a one sided finite difference scheme on the boundaries such that the leading order error term is the same as the one used in the interior.

In our framework, we use the following second order finite difference scheme for the first derivative of a field ψ at an interior point i (where the leading order error term was written explicitly):

$$\psi_i' = \frac{\psi_{i+1} - \psi_{i-1}}{2h} - \frac{h^2}{6}\psi_i''' + \dots , \tag{6}$$

where ψ_{i+1} and ψ_{i-1} are the values of the field ψ at the points $i+1$ and $i-1$ respectively, and h is the grid spacing.

To match this leading order term of the error, we use the following one sided finite difference scheme for the derivative of f at the left and right boundary points respectively []:

$$\psi_i' = \frac{\psi_{i+3} - 4\psi_{i+2} + 7\psi_{i+1} - 4\psi_i}{2h} - \frac{h^2}{6}\psi_i''' + \dots \tag{7}$$

$$\psi_i' = \frac{4\psi_i - 7\psi_{i-1} + 4\psi_{i-2} - \psi_{i-3}}{2h} - \frac{h^2}{6}\psi_i''' + \dots \tag{8}$$

1.2.2 Interpolation at the Boundaries

Since we are interested in evolving the fields at null infinity, we must choose a boundary condition that allows the fields to freely propagate outwards. To do so, we use interpolation at the outer boundaries of our computational domain to fill the ghost points in those regions. This is done by using the following interpolation scheme:

$$\psi_i = 4\psi_{i-1} - 6\psi_{i-2} + 4\psi_{i-3} - \psi_{i-4} , \tag{9}$$

where ψ_i is the value of the field at the ghost point i, and ψ_{i-1}, ψ_{i-2}, ψ_{i-3} and ψ_{i-4} are the values of the field at the points $i-1$, $i-2$, $i-3$ and $i-4$ respectively.

1.2.3 Evans Method

When dealing with operators like the Laplacian in spherical coordinates, we find some formal singularities which need to be removed in order for our code to work. To remove those singularities, we can apply the Evans Method. This method consists of rewriting the singular terms as a different differential operator, called the Evans operator, which can be evaluated at the grid points. The Evans operator is defined as

$$\partial_r\psi + \frac{p}{r}\psi = (p+1)\frac{d(r^p\psi)}{dr^{p+1}} , \tag{10}$$

where p is a constant. This operator can be expressed in terms of the grid points as

$$(p+1)\frac{d(r^p\psi)}{dr^{p+1}} = (\tilde{D}\psi)_i = (p+1)\frac{r_{i+1}^p\psi_{i+1} - r_{i-1}^p\psi_{i-1}}{r_{i+1}^{p+1} - r_{i-1}^{p+1}} , \tag{11}$$

where the subscripts $i+1$ and $i-1$ denote the grid points $i+1$ and $i-1$ respectively.

2 Wave Equation in 1+1 Dimensions

We start by considering the wave equation in 1+1 dimensions

$$\Box\psi \equiv -\partial_T^2\psi + \partial_X^2\psi = 0 . \tag{12}$$

From my previous work on the subject [], we concluded that we should use systems of equations that are first order both in space and in time, since the second order in space and first order in time

scheme proved to be problematic. Thus, we proceed to do a first order reduction of the wave equation by defining $\Pi \equiv -\partial_T \psi$, obtaining

$$\begin{cases} \partial_T \psi = -\Pi \\ \partial_T \Pi = -\partial_{\underline{i}} \partial^{\underline{i}} \psi \end{cases} . \tag{13}$$

We can add an additional constraint $C_{\underline{i}} = \partial_{\underline{i}} \psi - \Phi_{\underline{i}} \overset{!}{=} 0$ to our system of equations, to which small violations could be allowed. Using the time derivative of this constraint as an evolution equation for Φ and expressing the small violation of this constraint as $\gamma_2 C_{\underline{i}}$, where γ_2 is a small parameter corresponding to the allowed violation, we get

$$\begin{cases} \partial_T \psi = -\Pi \\ \partial_T \Phi = -\partial_X \Pi + \gamma_2 \, \partial_X \psi - \gamma_2 \, \Phi \\ \partial_T \Pi = -\partial_X \Phi \end{cases} . \tag{14}$$

We then proceed to make a coordinate change from inertial Minkowski coordinates to hyperboloidal coordinates. Addicionally, even though we could allow for small violations of our constraint, we will not. Thus, we set $\gamma_2 = 0$, obtaining the final form of our system of equations:

$$\begin{cases} \partial_t \psi = -\Pi \\ \partial_t \Phi = \mathcal{A} \, \left(H' \, \partial_x \Phi + \partial_x \Pi \right) \\ \partial_t \Pi = \mathcal{A} \, \left(H' \, \partial_x \Pi + \partial_x \Phi \right) \end{cases} , \tag{15}$$

where we defined $\mathcal{A}(x) = \frac{\Omega^2(x)}{L(x)(H'^2(x)-1)}$, and dropped the explicit dependences on x to simplify the notation.

We can now solve this system of equations using the aforementioned code, using truncation error matching for the derivatives on the boundaries and turning off the artificial dissipation on those points. Using that framework and giving the initial conditions

$$\psi(0,x) = A \, e^{-C \, x^2/2} \, , \quad \Phi(0,x) = -A \, C \, x \, \frac{\Omega^2(x)}{L(x)} \, e^{-C \, x^2/2} \quad \text{and} \quad \Pi(0,x) = 0 \, , \tag{16}$$

with $A = 1$ and $C = 100$, we obtain the evolution present in figure 3. In that evolution, it is noticeable that after the wave leaves the grid, we are left with a permanent negative displacement on our field. Even though this result is counterintuitive, it was proven in [] to be correct.

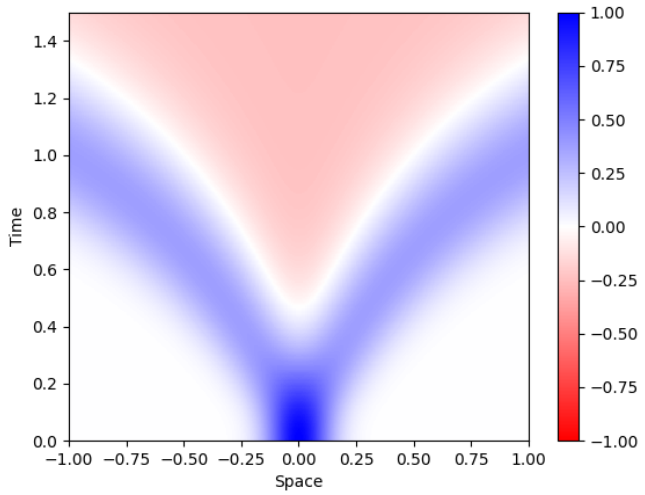

FIGURE 3: Evolution of the wave equation in 1+1 dimensions using hyperboloidal coordinates with the initial conditions given in equation (16), with $A = 1$ and $C = 100$.

Doing a norm convergence test (using the L^2 norm), we obtain a clean second order convergence during the whole evolution, as can be seen for ψ in the left of figure 4. We can also see that these results stay promising up until $\mathscr{I}$ through the pointwise convergence at that point, represented in the right of figure 4.

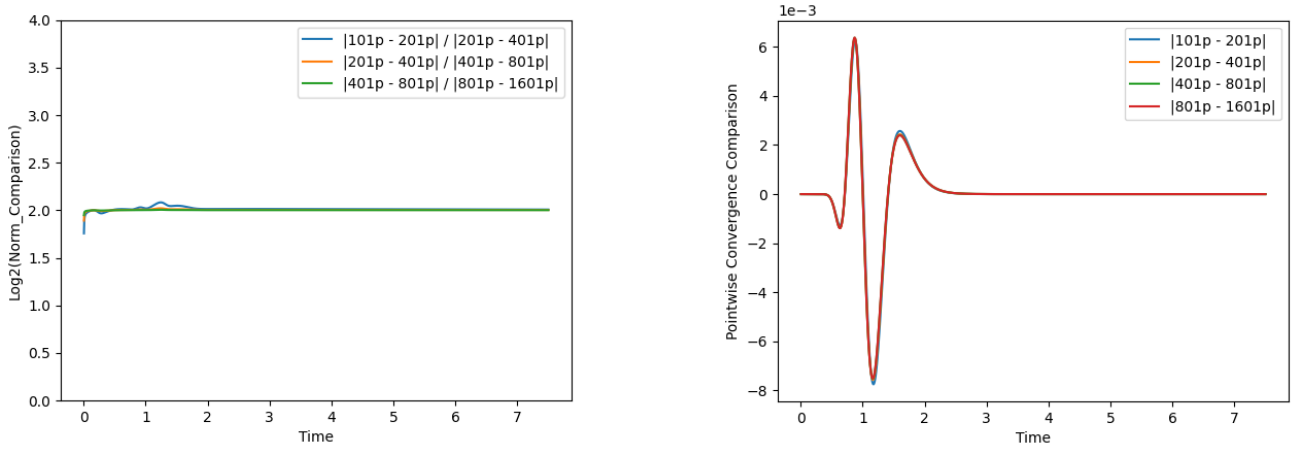

FIGURE 4: Convergence tests of the evolution of the wave equation in 1+1 dimensions using hyperboloidal coordinates, provided the initial conditions given in equation 16, with $A = 1$ and $C = 100$. On the left, we have the L^2 norm convergence, and on the right, we have the pointwise convergence at $\mathscr{I}$.

3 Wave Equation in 3+1 Dimensions With Spherical Symmetry

Now, let us consider the wave equation in 3+1 dimensions with spherical symmetry

$$\Box\psi \equiv -\partial_T^2\psi + \frac{1}{R^2}\partial_R\left(R^2\partial_R\psi\right) = 0\,. \tag{17}$$

Since ψ is a solution to this equation, it will decay at a rate of $1/R$, which is a problem because we want to know how our field behaves at $\mathscr{I}$. Thus, we need to renormalize this field in such a way that it does not vanish at infinity. With this in mind, let us define a new field Ψ such that

$$\Psi \equiv \chi\,\psi\,,$$

where we will take $\chi = \sqrt{1+R^2}$.

Applying that transformation to the wave equation, it becomes

$$\partial_T^2\Psi = \partial_R^2\Psi + \frac{2}{R(R^2+1)}\partial_R\Psi - \frac{3}{(R^2+1)^2}\Psi\,, \tag{18}$$

to which we can apply a first order reduction, obtaining

$$\begin{cases} \partial_T\Psi = -\Pi \\ \partial_T\Phi = -\partial_R\Pi + \gamma_2\partial_R\Psi - \gamma_2\Phi \\ \partial_T\Pi = -\partial_R\Phi - \frac{2}{R(R^2+1)}\Phi + \frac{3}{(R^2+1)^2}\Psi \end{cases}. \tag{19}$$

Doing a coordinate change from inertial Minkowski coordinates to hyperboloidal coordinates and setting $\gamma_2 = 0$ as we did previously, we get

$$\begin{cases} \partial_T \Psi = -\Pi \\ \partial_T \Phi = \mathcal{B}\left((r^2+\Omega^2)^2\left(H'\partial_r\Phi + \partial_r\Pi\right) + H'L\Omega\left(2r\Phi - 3\Omega\Psi + 2r^{-1}\Omega^2\Phi\right)\right) \\ \partial_T \Pi = \mathcal{B}\left((r^2+\Omega^2)^2\left(\partial_r\Phi + H'\partial_r\Pi\right) + L\Omega\left(2r\Phi - 3\Omega\Psi + 2r^{-1}\Omega^2\Phi\right)\right) \end{cases}, \tag{20}$$

where we defined $\mathcal{B} = \frac{\Omega^2}{L(H'^2-1)(r^2+\Omega^2)^2}$.

We can see that in our evolution equations for Φ and for Π, we have a term that is formally singular, to which we will need to apply the Evans method. For that, we rewrite those evolution equations, obtaining

$$\begin{cases} \partial_T \Psi = -\Pi \\ \partial_T \Phi = \mathcal{B}\left((r^2+\Omega^2)^2\left(H'\partial_r\Phi + \partial_r\Pi\right) + H'L\Omega\left(2r\Phi - 3\Omega\Psi - \Omega^2\partial_r\Phi\right) + H'L\Omega^3\left(\partial_r\Phi + 2r^{-1}\Phi\right)\right) \\ \partial_T \Pi = \mathcal{B}\left((r^2+\Omega^2)^2\left(\partial_r\Phi + H'\partial_r\Pi\right) + L\Omega\left(2r\Phi - 3\Omega\Psi - \Omega^2\partial_r\Phi\right) + L\Omega^3\left(\partial_r\Phi + 2r^{-1}\Phi\right)\right) \end{cases}, \tag{21}$$

where it is easy to see that we can apply the Evans method to the last terms in parenthesis.

Imposing the parity of each field at the origin and doing extrapolation at $\mathscr{I}$ (instead of truncation error matching that we used before) as our boundary conditions and using the initial data

$$\psi(0,r) = A\, e^{-C\, r^2/2}\,, \quad \Phi(0,r) = -A\, C\, r\, \frac{\Omega^2(r)}{L(r)}\, e^{-C\, r^2/2} \quad \text{and} \quad \Pi(0,r) = 0\,, \tag{22}$$

with $A = 1$ and $C = 100$, we obtain the evolution represented in figure 5.

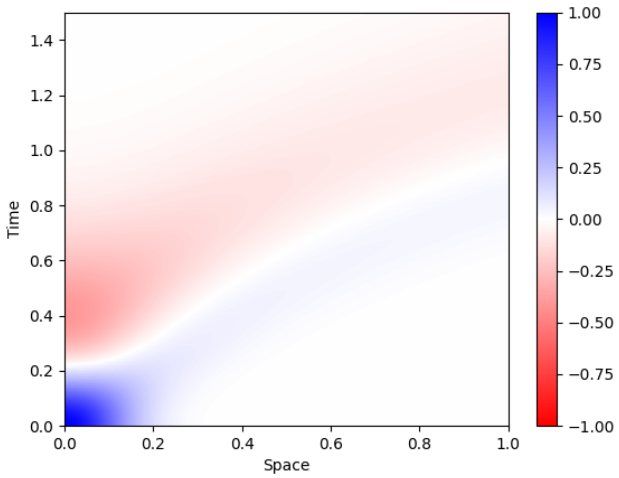

FIGURE 5: Evolution of the wave equation in 3+1 dimensions with spherical symmetry using hyperboloidal coordinates with the initial conditions given in equation (22), with $A = 1$ and $C = 100$.

Similarly to before, we obtain a clean second order convergence during the whole evolution, as can be seen for ψ in the left of figure 6. Addicionally, we still have very good pointwise convergence at $\mathscr{I}$, as can be seen in the right of figure 6. Despite the fact that these results are already very good, they could be further improved by doing truncation error matching at the outer boundary instead of the extrapolation that was used.

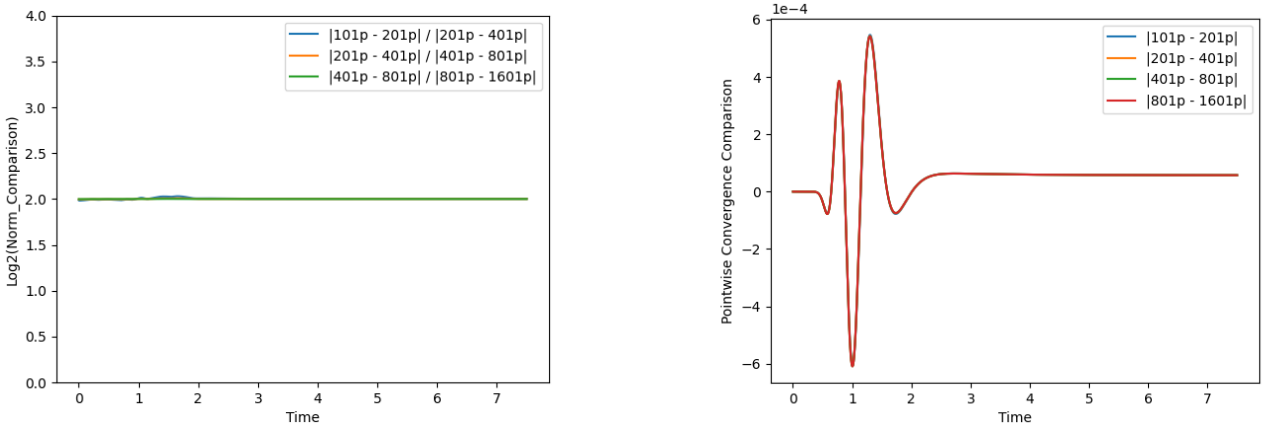

FIGURE 6: Convergence tests for the evolution for the wave equation in 3+1 dimensions with spherical symmetry using hyperboloidal coordinates, provided the initial conditions given in equation (22), with $A = 1$ and $C = 100$.. On the left, we have the L^2 norm convergence, and on the right, we have the pointwise convergence at $\mathscr{I}$.

4 Cubic Wave Equation in 3+1 Dimensions With Spherical Symmetry

Now it is time to tackle non-linear variations of the wave equation in 3+1 dimensions with spherical symmetry. We start by writing the wave equation as

$$\Box\psi \equiv -\partial_T^2\psi + \frac{1}{R^2}\partial_R\left(R^2\partial_R\psi\right) = \mathcal{X}\ , \tag{23}$$

where $\mathcal{X}$ is the non-linear term of our equation. Doing a first order reduction followed by the coordinate change to hyperboloidal coordinates, we get

$$\begin{cases} \partial_T\Psi = -\Pi \\ \partial_T\Phi = \mathcal{B}\left((r^2+\Omega^2)^2\left(H'\partial_r\Phi + \partial_r\Pi\right) + H'L\Omega\left(2r\Phi - 3\Omega\Psi + 2r^{-1}\Omega^2\Phi\right)\right) + \frac{H'\sqrt{2L}}{H'^2-1}\mathcal{X} \\ \partial_T\Pi = \mathcal{B}\left((r^2+\Omega^2)^2\left(\partial_r\Phi + H'\partial_r\Pi\right) + L\Omega\left(2r\Phi - 3\Omega\Psi + 2r^{-1}\Omega^2\Phi\right)\right) + \frac{\sqrt{2L}}{H'^2-1}\mathcal{X} \end{cases}\ , \tag{24}$$

where we used the previous definition for $\mathcal{B}$. We can now substitute $\mathcal{X} = (\Psi/\chi)^3$ to obtain the cubic wave equation.

Differently from the linear case, where we expect gaussian initial conditions that only differ by amplitude to behave similarly, in the non linear case, we expect that parameter to highly influence the solution. We will investigate this by solving the cubic wave equation with different initial conditions and comparing the results. Solving the cubic wave equation using the same boundary conditions as in the linear case, and using the initial conditions

$$\psi(0,r) = A\,e^{-C\,r^2/2}\ ,\quad \Phi(0,r) = -A\,C\,r\,\frac{\Omega^2(r)}{L(r)}\,e^{-C\,r^2/2}\quad\text{and}\quad \Pi(0,r) = 0\ , \tag{25}$$

with $A = 1.0$ for one of the runs and $A = 10.0$ for the other, while keeping $C = 10$ we get the results shown in figure 7. We can see that, for $A = 1$, we get a solution that behaves very similarly to the linear case, as the wave starts to disperse. Differently from the linear case however, it takes longer to disperse as there is a source term. For $A = 10$, we get a solution that grows rapidly until it explodes.

Despite this rapid grouth, our solution still converges cleanly both in the norm and pointwise convergence up until the analytical blowup. This is shown in figure 8 for the case where $A = 10$.

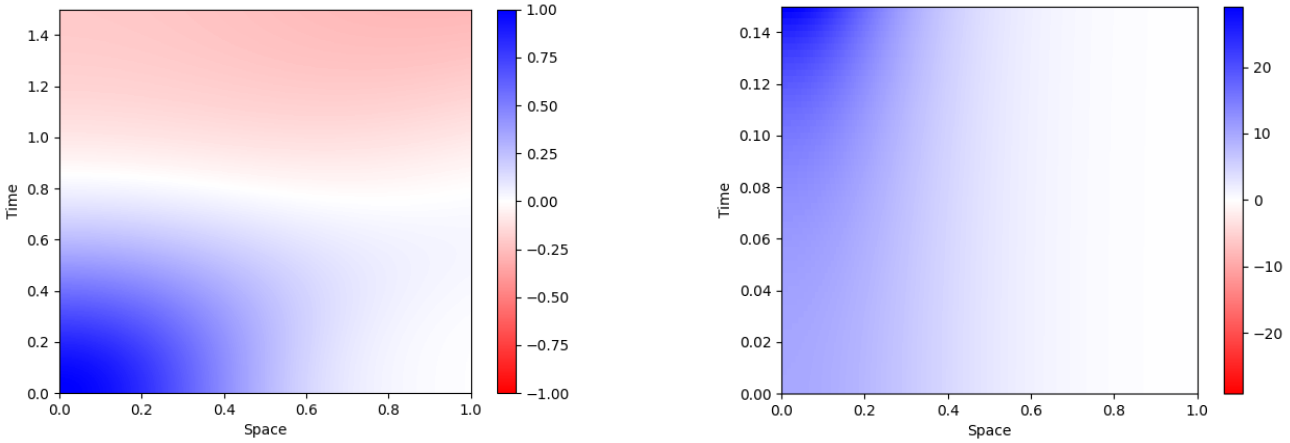

FIGURE 7: Evolution of the cubic wave equation in 3+1 dimensions with spherical symmetry using hyperboloidal coordinates with the initial conditions given in equation (25). On the left, we have $A = 1$ and $C = 10$. On the right, we have $A = 10$ and $C = 10$.

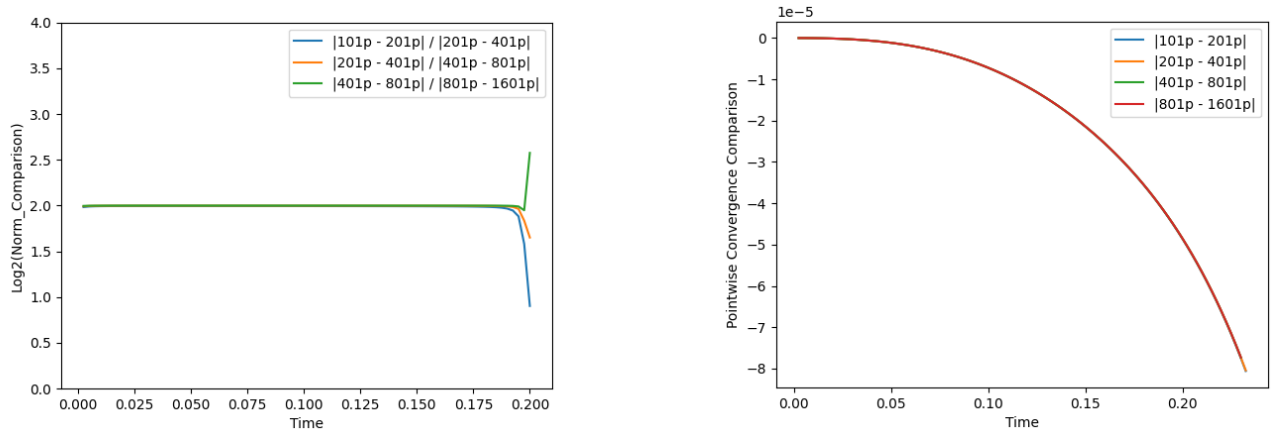

FIGURE 8: Convergence tests of the evolution of the cubic wave equation in 3+1 dimensions with spherical symmetry using hyperboloidal coordinates, provided the initial conditions given in equation (25), with $A = 10$ and $C = 10$. On the left, we have the L^2 norm convergence, and on the right, we have the pointwise convergence at $\mathscr{I}$.

5 Incoming Waves in Hyperboloidal Coordinates

As seen previously, when using hyperboloidal coordinates we expect incoming waves to be hard to resolve, as the error assiciated with them is expected to grow very rapidly as the wave prepagates. We will try to quantify that error by using incoming waves as initial conditions and comparing the numerical solution with the exact solution. It is then possible to study how much the error grows with the distance traveled towards the origin by doing several runs with the starting pulse further and further away.

First, we must build initial conditions that are purely incoming. We do that by doing a linear combination of an incoming and an outgoing wave, while making sure that the solution decays with $1/R$, that is

$$\psi(T, R) = \frac{f(T + R) - f(T - R)}{R}, \tag{26}$$

where we can freely choose the function f. By choosing f in such a way that in our domain, the outgoing wave vanishes. We will therefore choose f to be a gaussian pulse given by

$$f(x) = e^{-C(x-x_0)^2/2}, \tag{27}$$

where x_0 shiftes the center of the pulse and C determines the width of the pulse and we will consider $C = 100$. Thus, the full set of initial conditions is

$$\psi(T,R) = \frac{f(T+R)-f(T-R)}{R} \quad \Phi(T,R) = -\frac{f'(T+R)-f'(T-R)}{R} \quad \Pi(T,R) = \frac{(f'(T+R)-f'(T-R))R-(f(T+R)-f(T-R))}{R^2}, \tag{28}$$

where f' is the derivative of f. We now apply the change to hyperboloidal coordinates (where we defined a slightly modified height function $H(R) = \sqrt{S^2+R^2} - S$ in order to make t and T coincide at $R = 0$) and run several simulations for the wave equation in 3+1 dimensions with spherical symmetry (without applying the rescaling of the fields) up until the center of the pulse reaches the origin, while ranging x_0 from 1 to 10. The initial conditions for each pulse and the variation in time of the norm of the exact error normalized to the norm of the solution can be found in figure 9.

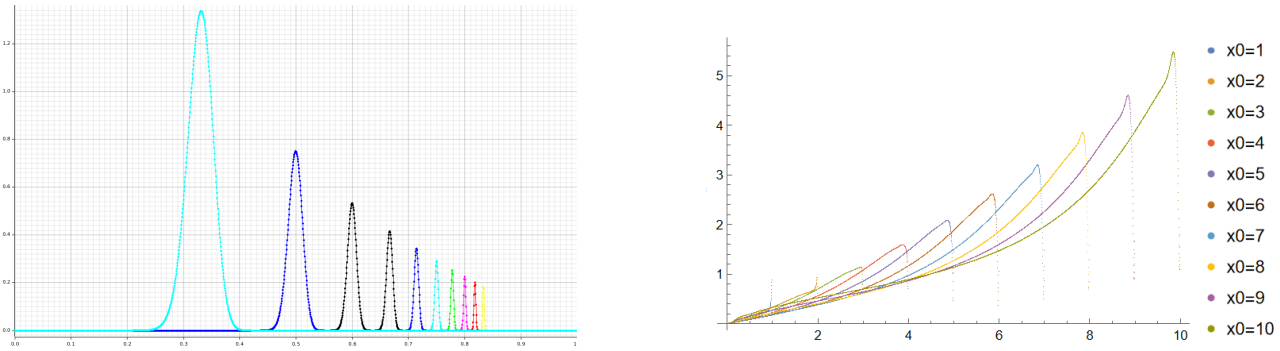

FIGURE 9: Evolution of the cubic wave equation in 3+1 dimensions with spherical symmetry using hyperboloidal coordinates with the initial conditions given in equation (25). On the left, we have $A = 1$ and $C = 10$. On the right, we have $A = 10$ and $C = 10$.

We can see just by the initial conditions that, in fact incoming waves become harder to resolve the further away they are, as in our initial conditions the gaussian gets thinner as it approaches $\mathscr{I}$. Addicionally, we can see that the error increases very rapidly as the waves propagate. Both these results were what we would expect to happen for this coordinate system. Therefore, if on our system we expect to have incoming waves, we should modify the coordinates to have a traditional Cauchy slice for part of the domain and then join that slice to a hyperboloidal slice when we don't expect to have incoming waves anymore.

6 Conclusions

Throughout this work, hyperboloidal coordinate system proved to be a very useful tool when studying the behaviour of outgoing waves, compactifying our domain while keeping the characteristic speeds of the waves finite. Our numerical experiments demonstrated the reliability of our code framework when dealing with different variations of the wave equation in this coordinate system, by showing clean second order convergence in all the performed simmulations.

However, this choice of coordinates is not adequate when there are incoming waves in our problem, since they are very hard to resolve and are great sources of error in the simulations. This suggests that a hybrid approach may be ideal for the cases where we expect to have incoming waves in a small portion of our domain, incorporating traditional Cauchy slices alongside hyperboloidal ones.

The master thesis that follows this work, will be focused on expanding the well estalished numerical relativity code *BAMPS*, making it able to perform simmulations in this coordinate system. In addition, more intricate non linearities will be studied, as we try to get closer to being able to solve the Einstein equations numerically.